



HAL
open science

Monoclinic–Orthorhombic Phase Transition with a Positive Volume Change in the Siliceous Zeolite Mobil-Five Induced by the High-Pressure Insertion of Dense Fluid Helium

Mario Santoro, Weiwei Dong, Konstantin Glazyrin, Julien Haines

► **To cite this version:**

Mario Santoro, Weiwei Dong, Konstantin Glazyrin, Julien Haines. Monoclinic–Orthorhombic Phase Transition with a Positive Volume Change in the Siliceous Zeolite Mobil-Five Induced by the High-Pressure Insertion of Dense Fluid Helium. *Journal of Physical Chemistry C*, 2021, 125 (43), pp.24249-24253. 10.1021/acs.jpcc.1c07791 . hal-03448360

HAL Id: hal-03448360

<https://hal.umontpellier.fr/hal-03448360>

Submitted on 19 Jul 2022

HAL is a multi-disciplinary open access archive for the deposit and dissemination of scientific research documents, whether they are published or not. The documents may come from teaching and research institutions in France or abroad, or from public or private research centers.

L'archive ouverte pluridisciplinaire **HAL**, est destinée au dépôt et à la diffusion de documents scientifiques de niveau recherche, publiés ou non, émanant des établissements d'enseignement et de recherche français ou étrangers, des laboratoires publics ou privés.

Monoclinic-Orthorhombic Phase Transition with a Positive Volume Change in the Siliceous Zeolite MFI Induced by the High-Pressure Insertion of Dense Fluid Helium

Mario Santoro^{‡,§}, Weiwei Dong^{||,¶}, Konstantin Glazyrin^{||}, Julien Haines^{*†}

[‡]Istituto Nazionale di Ottica, CNR-INO, 50019 Sesto Fiorentino, Italy.

[§]European Laboratory for Non Linear Spectroscopy (LENS), 50019 Sesto Fiorentino, Italy.

^{||}Deutsches Elektronen-Synchrotron, D-22607 Hamburg, Germany.

[¶]Beijing Synchrotron Radiation Facility, Institute of High Energy Physics, Chinese Academy of Sciences, Beijing, 100049, People's Republic of China.

[†]ICGM, CNRS, Université de Montpellier, ENSCM, 34095 Montpellier, France.

ABSTRACT

Synchrotron x-ray diffraction was used to investigate the insertion of helium in the archetypal siliceous zeolite Mobile-Five (MFI). Due to the very high degree of helium penetration into the pores and the framework, the monoclinic form of MFI is stabilized over a large pressure interval and the compressibility is much lower than when the pores are empty or filled with any other guest molecules or atoms except hydrogen. The structure of MFI transformed from monoclinic $P2_1/n$ to orthorhombic $Pnma$ with a discontinuous volume *increase* of 3% at pressures close to 10 GPa due to the filling process. The material is highly strained at pressures above 42 GPa, but remains crystalline. The strain is released on decompression and highly crystalline material is recovered.

1. Introduction

Helium has been found to easily penetrate the frameworks of certain forms of silica at high pressure such as α -cristobalite¹⁻² and silica glass³⁻⁷, resulting in swelling of the structure. Such behavior does not occur on compression in argon⁷, but can occur with slow kinetics above a threshold pressure in the case of the intermediate-sized neon atom⁶. In the case of porous, pure silica zeolites, larger atoms and molecules readily enter the pores at high pressure⁸⁻²⁴. In the case of the archetypal all-silica zeolite, silicalite-1 with the monoclinic Mobile-Five (MFI) structure and a three-dimensional pore system²⁵⁻²⁶, argon or simple molecules such as water, nitrogen and carbon dioxide can completely fill the pores system, but do not enter the framework^{8, 18, 22}. The exception is hydrogen²³, which has very recently been found to enter the secondary building units of the framework. The structure of MFI²⁵⁻²⁶ is formed by linear 5.3 Å x 5.6 Å channels along the **b** direction and 5.1 Å x 5.5 Å sinusoidal pores in the *xz* plane (Figure 1). High silica, MFI undergoes a ferroelastic phase transition²⁷ from the monoclinic $P2_1/n$ to the orthorhombic $Pnma$ form at 349 K. A similar phase transition is also observed at high pressure in the vicinity of 1 GPa⁸. When siliceous MFI is compressed in penetrating medium, such as H₂O or CO₂, this transition can occur at even lower pressures^{20, 22}. Filling with guest species was also found to stabilize the orthorhombic phase with respect to pressure-induced amorphization at very high pressures^{8, 18, 23}. In H₂-filled MFI²³, the crystalline phase is still observed at 60 GPa.

In the present work, we explore siliceous MFI with a focus on the effect of helium insertion into the monoclinic and orthorhombic phases, their stability fields as well as the volume changes and compressibility of this material.

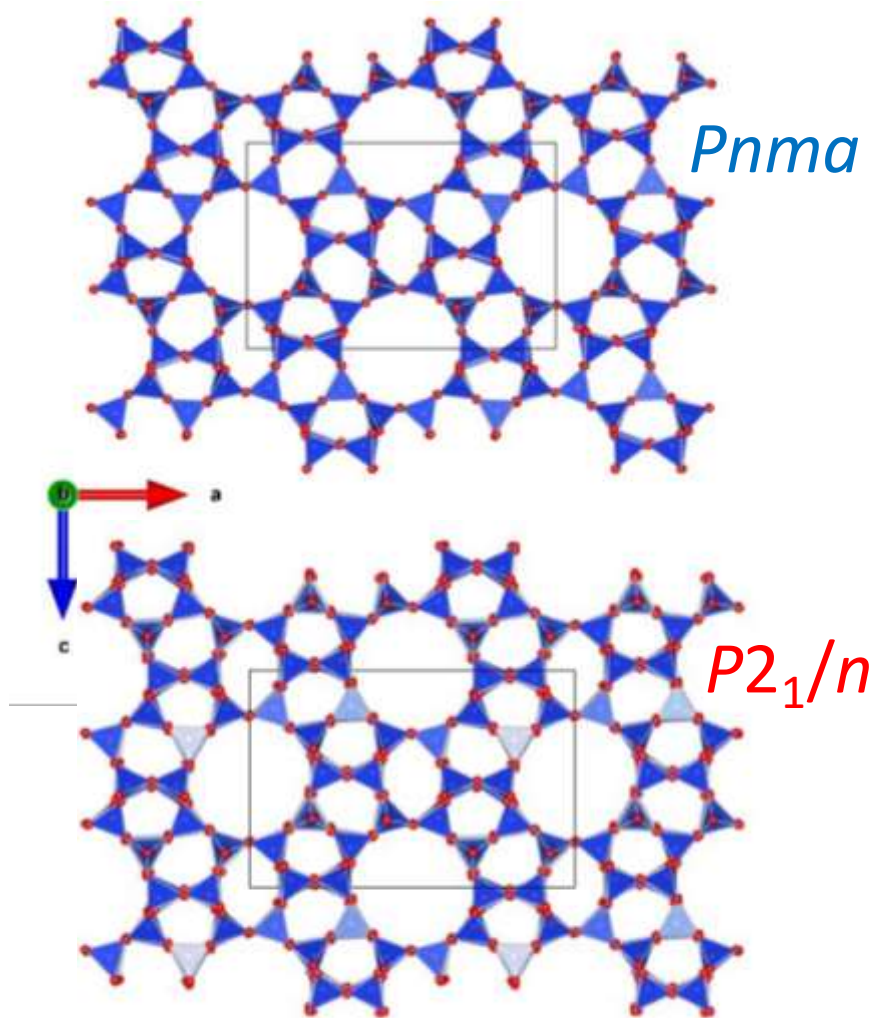


Figure 1. Structures of monoclinic $P2_1/n11$, Space Group 14 (below) and orthorhombic $Pnma$, S.G. 62 MFI (above). Comparing the structures, we note that the monoclinic form has $\alpha=90.6207^\circ$, and some small differences are observed in the Si-O-Si bridging angles. The unit cell of the monoclinic form is described in the non-standard space group setting in order to conserve the basis similar to the orthorhombic phase.

2. Methods

Calcined siliceous MFI, silicalite-1, was prepared by the sol-gel route in a fluoride medium followed by crystallization under hydrothermal conditions and then calcination as described previously²². The sample was placed in the hole of a gasket in a membrane diamond anvil cell

along with a ruby sphere used as a pressure sensor²⁸. Fluid helium was introduced at high pressure and the cell was closed at 0.13 GPa. Angle-dispersive x-ray powder diffraction measurements were performed at the extreme conditions beamline P02.2²⁹ of the PETRA-III synchrotron at DESY using monochromatic radiation with a wavelength of 0.4828 Å. The focused beam spot dimensions were 9 µm × 3 µm. Detection was performed with a Perkin Elmer XRD1621 (2048 x 2048 pixels, 200 µm x 200 µm) detector. The 2-D diffraction images were integrated, and then 1-D diffraction profiles were obtained using the program Dioptas³⁰. Le Bail refinements to obtain precise lattice parameters and volumes were performed using the program Fullprof³¹. The pressure was measured using the ruby fluorescence method²⁸.

3. Results and discussion

At ambient pressure, the sample adopted the known monoclinic structure for calcined MFI²⁶. Upon loading with helium at 0.13 GPa, the structure remained monoclinic, however, in contrast, to previous work on empty MFI^{8, 32-33} and MFI filled with many atoms of molecules, such as H₂O²² and CO₂²⁰, transformation to the more symmetrical orthorhombic *Pnma* was not observed below 1 GPa in spite of pore filling. In fact, even up to 9.1 GPa, the unit cell remained monoclinic with a clear splitting of *hkl* and *hk̄l* reflections (Figures 2 and 3). The monoclinic angle α was not found to decrease with pressure indicating no obvious tendency towards the orthorhombic form (Table 1, Figure 4). The unit cell of the monoclinic form is described in the non-standard *P2₁/n11*, S.G. 14 space group setting to conserve the same reference as the *Pnma* orthorhombic phase. The relative unit cell volume in the case of He filling is much higher than for the orthorhombic phases of empty³³ or Ar or CO₂-filled MFI⁸, resulting in a monoclinic MFI swelled with He (Figure 4). Helium is different from the other guest species mentioned above as it has been clearly shown to penetrate the frameworks of various silica forms such as silica glass³⁻⁵ and cristobalite¹ and thus can fill various rings and cages in the framework in addition to the 5.5 Å diameter pores. The situation is similar for H₂ and in the orthorhombic form of MFI

at high pressure, hydrogen molecules occupy the pores, but also the cages in the framework built up of 5- and 6-membered rings of SiO₄ tetrahedra¹⁹. In the case of H₂; however, measurements were not performed on the monoclinic form at low pressure and the monoclinic-orthorhombic phase transition was not investigated¹⁹. In another siliceous zeolite TON, insertion of H₂ at high pressure and high temperature was found to induce an anomalous volume increase and a phase transition to a higher symmetry structure²⁴.

The *a* lattice parameter decreases up to pressures of 7GPa, but between 7 and 9 GPa it is almost incompressible indicating the beginning of pre-transition phenomena (Figure 4). This is followed by major changes in the diffraction pattern at 10.9 GPa, which still in the fluid phase and more than 1 GPa below the solidification pressure of helium at 12.1 GPa,. At 10.9 GPa the peaks sharpen and shift to lower 2θ angles, the *hkl* reflections splittings disappear (e.g. $\bar{3}13$ and 313), and additionally *hkl* reflections merge with *khl* reflections. At this pressure, the unit cell parameters are $a = b = 19.443(2)$ Å and $c = 13.071(3)$ Å with accidentally the same values for *a* and *b*, even though from a structural point of view these directions are very different. This accidental equivalence is not new and it was previously observed for MFI in Ar and CO₂ at high pressure⁸. A volume *increase* of close to 3% is observed at the phase transition due to insertion of the dense fluid helium into the structure (Figure 5). A continuous or discontinuous decrease in monoclinic angle and volume should be expected for this monoclinic to orthorhombic, ferroelastic, phase transition at high pressure. The present behavior is clearly different from the previous reported cases due to the different nature of penetrating agent – He, which enters the voids in the framework of the crystal structure. Here, we also report that the *a* cell parameter is significantly more compressible in the orthorhombic phase of He-filled MFI, which corresponds to the direction of the sinusoidal pores. The *b* parameter along the direction of the linear pores is particularly stiff.

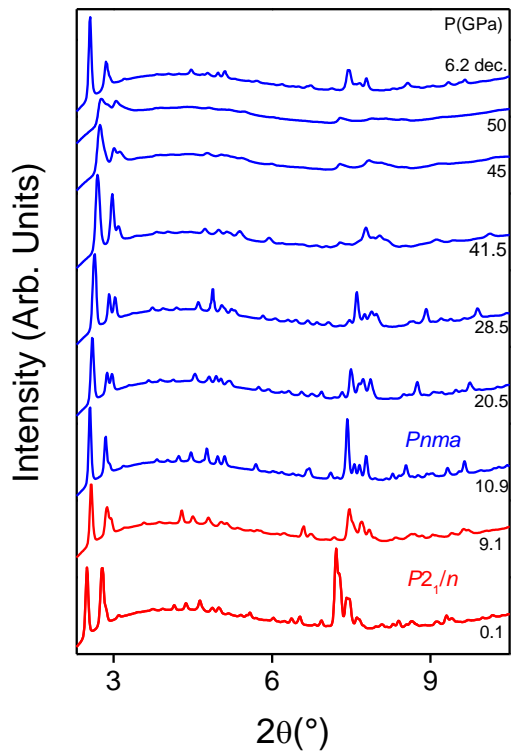


Figure 2. X-ray diffraction patterns of MFI in He as a function of pressure ($\lambda=0.4828$ Å). The data obtained on decompression are indicated by “dec.” label.

The peaks of MFI in helium remain very sharp up to 42 GPa due to the low degree of deviatoric stress of this quasihydrostatic pressure-transmitting medium (Figure 2). Above 42 GPa, broadening occurs linked to strain in the structure of MFI. The lines sharpen on pressure release, but we observe some hysteresis in structural behavior. After decompression to 6.2 GPa, the volume of MFI is similar to that observed on compression, but the structure remains orthorhombic.

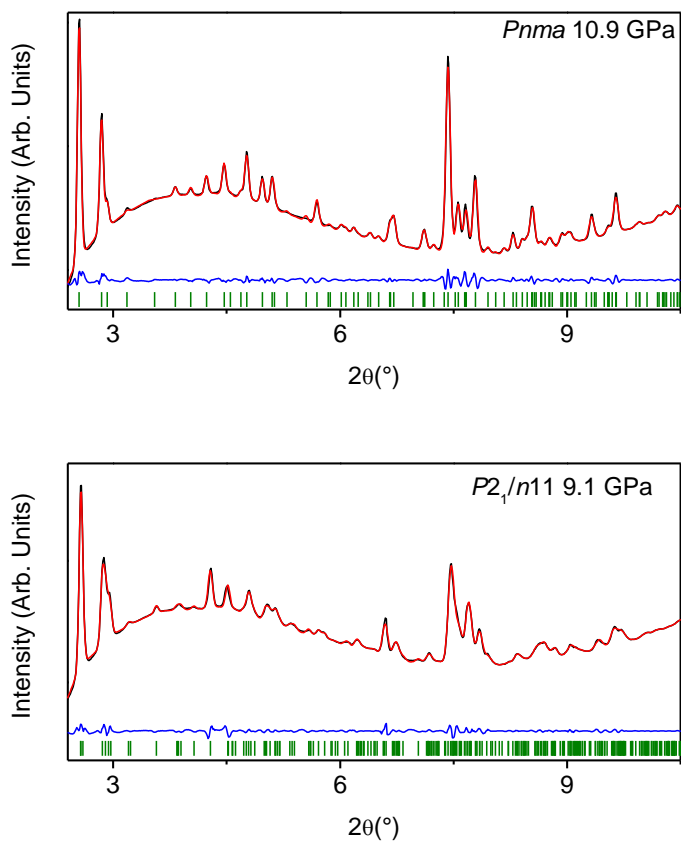


Figure 3. Experimental (black), calculated (red) and difference (blue) profiles ($\lambda=0.4828 \text{ \AA}$) for the Le Bail fits for the $P2_1/n$ structure of MFI/He at 9.1 GPa (below) and for the $Pnma$ structure of MFI/He at 10.9 GPa (above). Vertical bars indicate the calculated positions of the Bragg reflections.

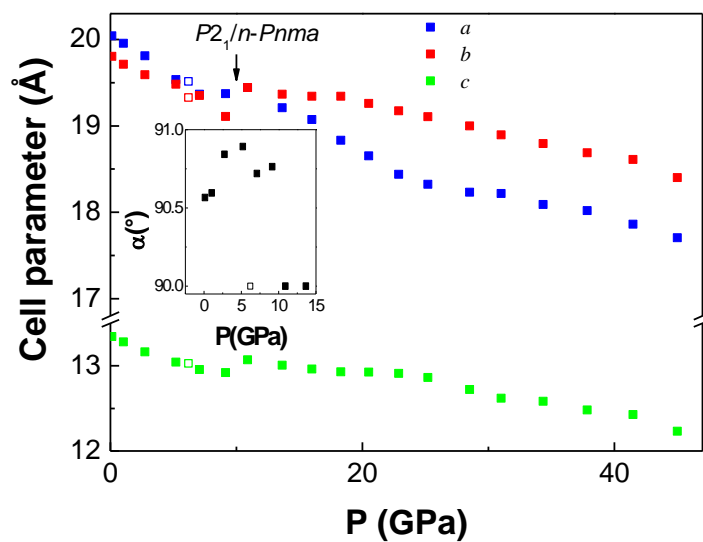


Figure 4. Cell parameters of MFI in He as a function of pressure on compression (solid symbols) and on decompression (empty symbols). Error bars are smaller than the symbol size.

Table 1. Unit cell parameters of monoclinic (space group $P2_1/n11$, S.G.14) and orthorhombic silicalite-1 (space group $Pnma$) in He as a function of pressure. The structural transition occurs between 9.1 and 10.9 GPa upon compression.

$P(\text{GPa})$	$a(\text{Å})$	$b(\text{Å})$	$c(\text{Å})$	$\alpha(^{\circ})$	$V(\text{Å}^3)$
0.13	20.042(3)	19.806(4)	13.344(5)	90.57(4)	5297(2)
1.03	19.956(5)	19.712(6)	13.281(8)	90.60(7)	5224(4)
2.74	19.812(6)	19.592(6)	13.164(5)	90.84(5)	5109(3)
5.2	19.54(1)	19.48(2)	13.043(5)	90.89(5)	4964(6)
7.1	19.37(2)	19.35(3)	12.956(6)	90.72(6)	4855(8)
9.1	19.373(5)	19.11(1)	12.919(4)	90.76(6)	4782(4)
10.9	19.443(2)	19.443(2)	13.071(3)	90	4941(1)
13.7	19.210(6)	19.366(3)	13.006(3)	90	4839(2)
16	19.074(6)	19.342(4)	12.963(3)	90	4783(2)
18.3	18.832(5)	19.344(3)	12.929(3)	90	4710(2)
20.5	18.653(9)	19.260(4)	12.927(4)	90	4644(3)
22.9	18.440(9)	19.173(4)	12.912(3)	90	4565(3)
25.2	18.322(6)	19.104(6)	12.863(3)	90	4502(3)
28.5	18.23(1)	18.999(4)	12.720(4)	90	4406(3)
31.0	18.216(8)	18.897(6)	12.620(4)	90	4344(3)
34.4	18.09(2)	18.794(6)	12.582(6)	90	4277(5)
37.9	18.02(2)	18.689(8)	12.481(7)	90	4202(6)
41.5	17.86(2)	18.610(4)	12.427(5)	90	4131(4)
45	17.70(2)	18.40(1)	12.23(1)	90	3984(7)
6.2 dec.	19.52(1)	19.327(6)	13.029(4)	90	4914(4)

Note that the empty starting material is monoclinic with $a=20.1344(1)\text{Å}$, $b=19.9018(1)\text{Å}$, $c=13.38641(8)\text{Å}$, $\alpha=90.6207(5)^{\circ}$ in the non-standard $P2_1/n11$ setting of the space group ($P2_1/n$, S.G. 14) in order to retain the same axes as the orthorhombic aristotype $Pnma$ ²²

In comparison to He-filled MFI, the diffraction lines are slightly broader in H₂-filled MFI, but a rapid increase was never observed and the broadening is more gradual. The unit cell is less compressible than in the case of He-filled MFI. As the He atoms and the hydrogen molecules are similar in size, the amount of helium in the MFI structure could be expected to be similar to that found in the case of H₂ from GCMC simulations²³ at pressures where the unit cell volumes are similar as for example, between 12 and 16 GPa, for which around 135 H₂ molecules were inserted per unit.

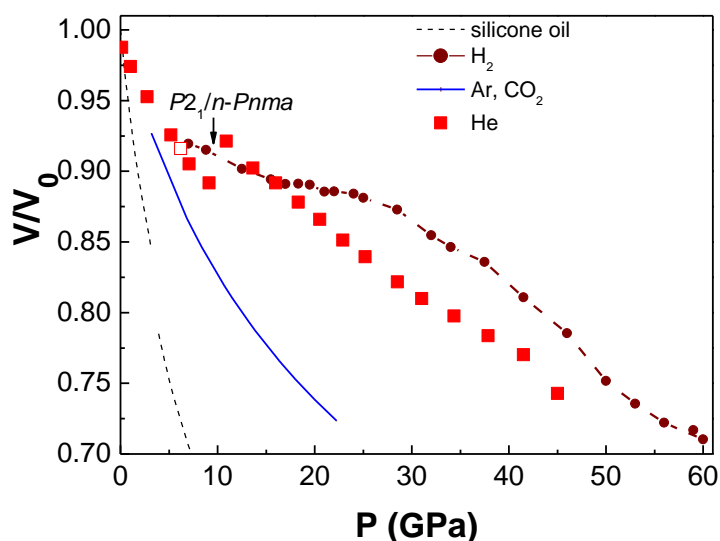


Figure 5. Relative volume (V/V_0) of MFI in He as a function of pressure on compression (solid squares) and on decompression (empty squares). Circles, dashed and solid lines represents the behavior of MFI in H₂¹⁹, silicone oil³³ and Ar and CO₂⁸, respectively. Error bars are smaller than the symbol size.

4. Conclusions

Helium readily fills the structure of monoclinic MFI, stabilizing this phase at pressures of ~10 GPa, which is much higher than reported for any other atomic or molecular guest species. Above this pressure, but still 1-2 GPa below the solidification pressure of helium, a transition

to the orthorhombic form is observed with a volume *increase* of about 3% due to further filling with dense fluid helium that completely changes the mechanism of this transition, which is normally ferroelastic in the absence of pore filling. Indeed, changes in the local structure of inserted helium, mimicking solidification-related changes in pure helium, are likely to occur and to be the driving force for the observed transition in He filled MFI.

1. Sato, T.; Takada, H.; Yagi, T.; Gotou, H.; Okada, T.; Wakabayashi, D.; Funamori, N., Anomalous Behavior of Cristobalite in Helium under High Pressure. *Phys. Chem. Miner.* **2013**, *40*, 3-10.
2. Matsui, M.; Sato, T.; Funamori, N., Crystal Structures and Stabilities of Cristobalite-Helium Phases at High Pressures. *Am. Mineral.* **2014**, *99*, 184-189.
3. Sato, T.; Funamori, N.; Yagi, T., Helium Penetrates into Silica Glass and Reduces Its Compressibility. *Nat. Commun.* **2011**, *2*, 345.
4. Shen, G. Y.; Mei, Q. A.; Prakapenka, V. B.; Lazor, P.; Sinogeikin, S.; Meng, Y.; Park, C., Effect of Helium on Structure and Compression Behavior of SiO₂ Glass. *Proc. Natl. Acad. Sci. USA* **2011**, *108*, 6004-6007.
5. Weigel, C.; Polian, A.; Kint, M.; Ruffle, B.; Foret, M.; Vacher, R., Vitreous Silica Distends in Helium Gas: Acoustic Versus Static Compressibilities. *Phys. Rev. Lett.* **2012**, *109*, 245504.
6. Coasne, B.; Weigel, C.; Polian, A.; Kint, M.; Rouquette, J.; Haines, J.; Foret, M.; Vacher, R.; Ruffle, B., Poroelastic Theory Applied to the Adsorption-Induced Deformation of Vitreous Silica. *J. Phys. Chem. B* **2014**, *118*, 14519-14525.
7. Weigel, C.; Foret, M.; Hehlen, B.; Kint, M.; Clement, S.; Polian, A.; Vacher, R.; Ruffle, B., Polarized Raman Spectroscopy of ν -SiO₂ under Rare-Gas Compression. *Phys Rev B* **2016**, *93*, 224303.
8. Haines, J.; Cambon, O.; Levelut, C.; Santoro, M.; Gorelli, F.; Garbarino, G., Deactivation of Pressure-Induced Amorphization in Silicalite SiO₂ by Insertion of Guest Species. *J. Am. Chem. Soc.* **2010**, *132*, 8860-8661.
9. Coasne, B.; Haines, J.; Levelut, C.; Cambon, O.; Santoro, M.; Gorelli, F.; Garbarino, G., Enhanced Mechanical Strength of Zeolites by Adsorption of Guest Molecules. *Phys. Chem. Chem. Phys.* **2011**, *13*, 20096-20099.
10. Santoro, M.; Gorelli, F.; Haines, J.; Cambon, O.; Levelut, C.; Garbarino, G., Silicon Carbonate Phase Formed from Carbon Dioxide and Silica under Pressure. *Proc. Natl. Acad. Sci. USA* **2011**, *108*, 7689-7692.
11. Santoro, M.; Gorelli, F. A.; Bini, R.; Haines, J.; van der Lee, A., High-Pressure Synthesis of a Polyethylene/Zeolite Nano-Composite Material. *Nat. Commun.* **2013**, *4*, 1557.

12. Scelta, D.; Ceppatelli, M.; Santoro, M.; Bini, R.; Gorelli, F. A.; Perucchi, A.; Mezouar, M.; van der Lee, A.; Haines, J., High Pressure Polymerization in a Confined Space: Conjugated Chain/Zeolite Nanocomposites. *Chem. Mater.* **2014**, *26*, 2249-2255.
13. Vezzalini, G.; Arletti, R.; Quartieri, S., High-Pressure-Induced Structural Changes, Amorphization and Molecule Penetration in MFI Microporous Materials: A Review. *Acta Crystallogr. B* **2014**, *70*, 444-451.
14. Santoro, M.; Dziubek, K.; Scelta, D.; Ceppatelli, M.; Gorelli, F. A.; Bini, R.; Thibaud, J.-M.; Di Renzo, F.; Cambon, O.; Rouquette, J.; et al., High Pressure Synthesis of All-Transoid Polycarbonyl [-(C=O)-](N) in a Zeolite. *Chem Mater* **2015**, *27*, 6486-6489.
15. Arletti, R.; Leardini, L.; Vezzalini, G.; Quartieri, S.; Gigli, L.; Santoro, M.; Haines, J.; Rouquette, J.; Konczewicz, L., Pressure-Induced Penetration of Guest Molecules in High-Silica Zeolites: The Case of Mordenite. *Phys. Chem. Chem. Phys.* **2015**, *17*, 24262-24274.
16. Richard, J.; Cid, S. L.; Rouquette, J.; van der Lee, A.; Bernard, S.; Haines, J., Pressure-Induced Insertion of Ammonia Borane in the Siliceous Zeolite, Silicalite-1F. *J. Phys. Chem. C* **2016**, *120*, 9334-9340.
17. Santoro, M.; Scelta, D.; Dziubek, K.; Ceppatelli, M.; Gorelli, F. A.; Bini, R.; Garbarino, G.; Thibaud, J.-M.; Di Renzo, F.; Cambon, O.; et al., Synthesis of 1D Polymer/Zeolite Nanocomposites under High Pressure. *Chem. Mater.* **2016**, *28*, 4065-4071.
18. Santoro, M.; Gorelli, F. A.; Bini, R.; Haines, J., Intermolecular Interactions in Highly Disordered, Confined Dense N₂. *J. Phys. Chem. Lett.* **2017**, *8*, 2406-2411.
19. Thibaud, J. M.; Rouquette, J.; Dziubek, K.; Gorelli, F. A.; Santoro, M.; Garbarino, G.; Clement, S.; Cambon, O.; van der Lee, A.; Di Renzo, F.; et al., Saturation, of the Siliceous Zeolite TON with Neon at High Pressure. *J. Phys. Chem. C* **2018**, *122*, 8455-8460.
20. Marqueno, T., Santamaria-Perez, D.; Ruiz-Fuertes, J.; Chulia-Jordan, R.; Jorda, J. L.; Rey, F.; McGuire, C.; Kavner, A.; MacLeod, S.; Daisenberger, D.; et al., An Ultrahigh CO₂-Loaded Silicalite-1 Zeolite: Structural Stability and Physical Properties at High Pressures and Temperatures. *Inorg. Chem.* **2018**, *57*, 6447-6455.
21. Santoro, M.; Dziubek, K.; Scelta, D.; Morana, M.; Gorelli, F. A.; Bini, R.; Hanfland, M.; Rouquette, J.; di Renzo, F.; Haines, J., Dense, Subnano Phase of Clustered O₂. *J. Phys. Chem. C* **2019**, *123*, 9651-9657.
22. Santoro, M.; Veremeienko, V.; Polisi, M.; Fantini, R.; Alabarse, F.; Arletti, R.; Quartieri, S.; Svitlyk, V.; van der Lee, A.; Rouquette, J.; et al., Insertion and Confinement of H₂O in Hydrophobic Siliceous Zeolites at High Pressure. *J. Phys. Chem. C* **2019**, *123*, 17432-17439.
23. Xu, W.; Liu, X. D.; Pena-Alvarez, M.; Jiang, H. C.; Dalladay-Simpson, P.; Coasne, B.; Haines, J.; Gregoryanz, E.; Santoro, M., High-Pressure Insertion of Dense H₂ into a Model Zeolite. *J. Phys. Chem. C* **2021**, *125*, 7511-7517.
24. Paliwoda, D.; Comboni, D.; Poreba, T.; Hanfland, M.; Alabarse, F.; Maurin, D.; Michel, T.; Demirci, U. B.; Rouquette, J.; di Renzo, F.; et al., Anomalous Volume Changes in the Siliceous Zeolite Theta-1 TON Due to Hydrogen Insertion under High-Pressure, High-Temperature Conditions. *J. Phys. Chem. Lett.* **2021**, *12*, 5059-5063.
25. Olson, D. H.; Kokotailo, G. T.; Lawton, S. L.; Meier, W. M., Crystal-Structure and Structure-Related Properties of ZSM-5. *J. Phys. Chem.* **1981**, *85*, 2238-2243.
26. Hay, D. G.; Jaeger, H., Orthorhombic Monoclinic Phase-Changes in ZSM-5 Zeolite Silicalite. *J. Chem. Soc.-Chem. Commun.* **1984**, 1433-1433.
27. Ardit, M.; Martucci, A.; Cruciani, G., Monoclinic-Orthorhombic Phase Transition in ZSM-5 Zeolite: Spontaneous Strain Variation and Thermodynamic Properties. *J. Phys. Chem. C* **2015**, *119*, 7351-7359.
28. Mao, H. K.; Xu, J.; Bell, P. M., Calibration of the Ruby Pressure Gauge to 800-Kbar under Quasi-Hydrostatic Conditions. *J. Geophys. Res.-Solid* **1986**, *91*, 4673-4676.

29. Liermann, H. P.; Konopkova, Z.; Morgenroth, W.; Glazyrin, K.; Bednarcik, J.; McBride, E. E.; Petitgirard, S.; Delitz, J. T.; Wendt, M.; Bican, et al., The Extreme Conditions Beamline P02.2 and the Extreme Conditions Science Infrastructure at Petra III. *J. Synchrotron. Rad.* **2015**, *22*, 908-924.
30. Prescher, C.; Prakapenka, V. B., Dioptas: A Program for Reduction of Two-Dimensional X-Ray Diffraction Data and Data Exploration. *High. Press. Res.* **2015**, *35*, 223-230.
31. Rodriguez-Carvajal, J., Magnetic Structure Determination from Powder Diffraction Using the Program Fullprof. *Appl. Crystallogr.* **2001**, 30-36.
32. Quartieri, S.; Arletti, R.; Vezzalini, G.; Di Renzo, F.; Dmitriev, V., Elastic Behavior of MFI-Type Zeolites: 3-Compressibility of Silicalite and Mutinaite. *J. Solid State Chem.* **2012**, *191*, 201-212.
33. Haines, J.; Levelut, C.; Isambert, A.; Hebert, P.; Kohara, S.; Keen, D. A.; Hammouda, T.; Andrault, D., Topologically Ordered Amorphous Silica Obtained from the Collapsed Siliceous Zeolite, Silicalite-1-F: A Step toward "Perfect" Glasses. *J. Am. Chem. Soc.* **2009**, *131*, 12333-12338.

TOC Graphic

